

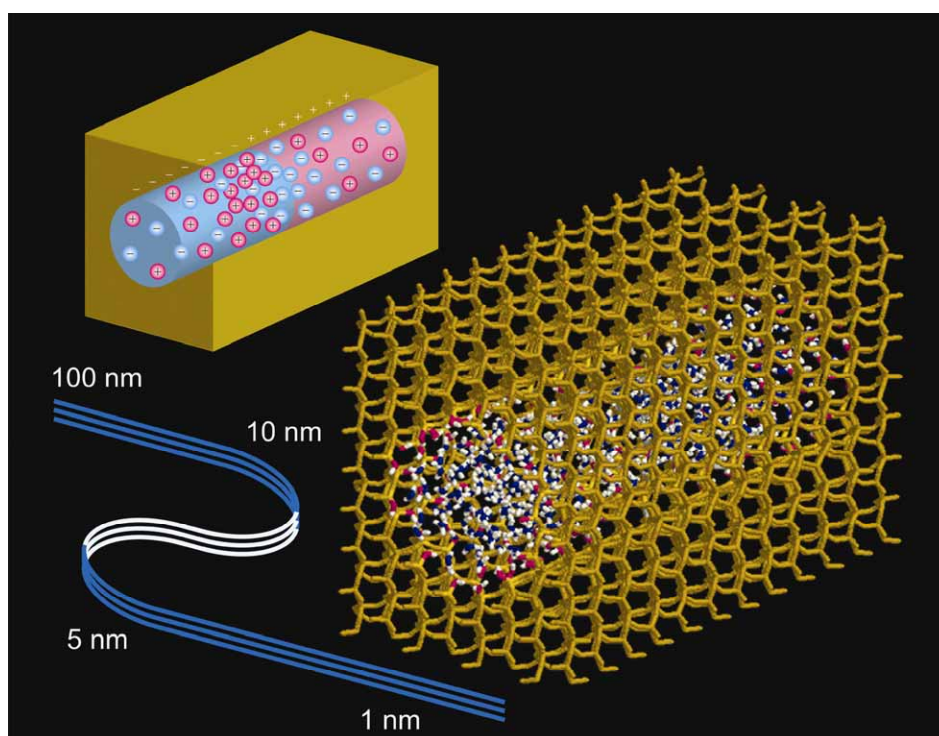
Chem Soc Rev

This article was published as part of the
**From microfluidic application to
nanofluidic phenomena issue**

Reviewing the latest advances in microfluidic and nanofluidic
research

Guest Editors Professors Albert van den Berg, Harold Craighead and Peidong Yang

Please take a look at the issue 3 [table of contents](#) to access
other reviews in this themed issue



Nanofluidics in chemical analysis†

Aigars Piruska,^a Maojun Gong,^b Jonathan V. Sweedler^b and Paul W. Bohn^{*a}

Received 3rd July 2009

First published as an Advance Article on the web 23rd October 2009

DOI: 10.1039/b900409m

Nanofluidic architectures and devices have already had a major impact on forefront problems in chemical analysis, especially those involving mass-limited samples. This *critical review* begins with a discussion of the fundamental flow physics that distinguishes nanoscale structures from their larger microscale analogs, especially the concentration polarization that develops at nanofluidic/microfluidic interfaces. Chemical manipulations in nanopores include nanopore-mediated separations, microsensors, especially resistive-pulse sensing of biomacromolecules, fluidic circuit analogs and single molecule measurements. Coupling nanofluidic structures to three-dimensional microfluidic networks is especially powerful and results in applications in sample preconcentration, nanofluidic injection/collection and fast diffusive mixing (160 references).

1. Introduction

Nanofluidics is a relatively new field; however phenomena that are relevant to nanofluidics and structures with nanometre size confinement were investigated long before the term nanofluidics was coined. The impetus for concentrating on nanofluidics as a distinct field stemmed from advances in microfabrication that enabled the construction of well controlled nanostructures, thus presenting new opportunities to refine our understanding of nanoscale processes and explore their use for chemical analysis. Manz *et al.*¹ may have been the first to recognize the advantages of miniaturized analysis systems. Since then considerable work has been done to demonstrate various

miniaturized components and systems for analysis on small length and volume scales. Several practical considerations drive the miniaturization of chemical analysis systems from macro- to micro- to nanoscale. Besides the obvious reduction of sample size and material consumption, the reduction in physical dimensions shortens analysis time due to enhanced mass transport, the characteristic time scale of which is proportional to l^2/D . Miniaturization down to the nanoscale begins to approach the natural scaling lengths of physical laws governing the behavior of molecular analytes. Exploring interaction between analyte and nanosystems, and improving molecular manipulation at this level provide us with new tools for chemical analysis and detection.

The special character of nanofluidics arises from the fact that several important length scales become comparable in these systems. The electric double layer (EDL), characterized by the inverse Debye length (κ), the cross-sectional dimension of a nanochannel and the size of molecules fall within the range 1 to 100 nm under typical conditions. Changing the

^a Department of Chemical and Biomolecular Engineering and Department of Chemistry and Biochemistry, University of Notre Dame, Notre Dame, IN 46556, USA. E-mail: pbohn@nd.edu

^b Department of Chemistry, University of Illinois at Urbana-Champaign, 600 S. Mathews Ave., Urbana, IL 61801, USA

† Part of the themed issue: From microfluidic application to nanofluidic phenomena.



Aigars Piruska

Aigars Piruska was born in Riga, Latvia, in 1979. He received his BS degree in chemistry from the University of Latvia, Riga, in 2001 and his PhD degree from the University of Cincinnati, Cincinnati, OH, in 2006. Currently, he is a Postdoctoral Researcher with the Department of Chemical Engineering, University of Notre Dame du Lac. His research interests include environmental sensing and micro-nanofluidics.



Maojun Gong

Maojun Gong received his BS in chemical physics from the University of Science and Technology of China in 1998 and his PhD in analytical chemistry from the University of Cincinnati in 2006. He worked as a postdoctoral research associate in the Department of Chemistry at the University of Illinois at Urbana-Champaign and is currently at the University of Michigan, Ann Arbor. His research is focused on microfluidic-nanofluidic instrumentation and technologies including microfabrication and characterization of microfluidic-nanofluidic devices and their applications in the analytical and bioanalytical field.

EDL or channel dimension can thus significantly affect molecular transport.

Reduction of channel size down to the nanoscale also causes a considerable increase in a surface-to-volume ratio. As a result surface processes are more pronounced. For example, the volume of a cylindrical nanochannel 100 nm in diameter and 1 μm in length is about 10 aL (or about $\sim 10^8$ water molecules). Even for this rather wide nanochannel, $\sim 2\%$ of all water molecules would be at the solid/liquid interface (for a nanochannel 10 nm in diameter, the fraction of water at interface would reach $\sim 20\%$). In addition, when the channel cross-section is of the order of the EDL, nanopore anion and cation concentrations are affected by surface charge and can significantly deviate from the bulk values.

A typical surface charge density ($\sim 2 \times 10^{-3} \text{ C m}^{-2}$) for the $100 \text{ nm} \times 1 \mu\text{m}$ nanochannel cited above would result in ~ 4000 electron charges on the interior wall of the nanochannel, requiring $\geq 1 \text{ mM}$ electrolyte concentration of counter-ions, just to balance the surface charge. Thus, ionic strength of the solution can be adjusted to control the relative populations of counter- and co-ions in the nanochannel. At low ionic strength (and significant EDL overlap) counter-ion concentration and nanochannel conductance are determined purely by surface charge density (see Fig. 1).² For common buffer concentrations (1 to 100 mM) used in analysis the inverse Debye lengths range from 10 to 1 nm. Small molecule diffusion times across such nanochannels are of the order of 10^{-5} to 10^{-4} s, which is advantageous for utilizing heterogeneous reactions within nanochannels. Adsorption (or desorption) of the surface monolayer ($\Gamma = 10^{-10}$ to $10^{-11} \text{ mol cm}^{-2}$) would cause the concentration to change $\sim 1\text{--}5 \text{ mM}$, indicating that selective capture and subsequent release within a nanochannel can be used for purification and concentration.

This review focuses on developments in nanofluidics pertinent to chemical analysis: studies that highlight unique

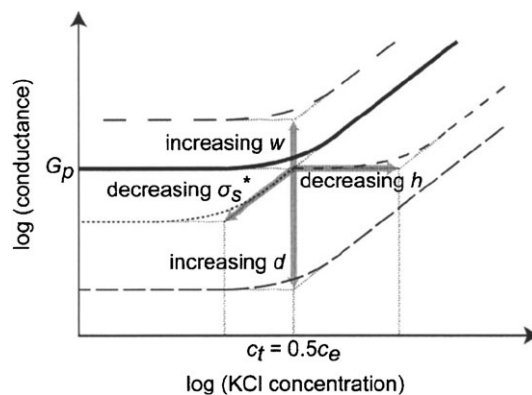


Fig. 1 Conductance of a nanochannel as a function of various nanochannel parameters. Reproduced with permission from ref. 2.

features of nanochannels— transport, detection and analysis in nanochannels and at micro/nanofluidic interfaces. In the Theoretical Background section transport within nanochannels and concentration polarization are discussed. Then various applications of nanofluidics are discussed: separations, translocation, and manipulation of species in nanochannels and nanopores, followed by work that utilizes unique features of nano–microchannel junctions. Some topics, such as fabrication of nanofluidic structures, are purposely omitted. Readers interested in other aspects of nanofluidics are referred to recent reviews addressing fabrication,^{3–5} wetting in nanostructures,⁶ transport,^{5,7–9} DNA analysis¹⁰ and linearization,¹¹ separations,^{8,12} and nanoscale lipid bilayer structures.¹³

2. Theoretical background

The first theoretical description of flow in nanofluidic channels was given by Rice and Whitehead¹⁴ who used the Debye–Hückel approximation which is valid for small ($< 50 \text{ mV}$) ζ -potentials. They studied electroosmosis, streaming current,



Jonathan V. Sweedler

Jonathan Sweedler received his PhD (University of Arizona) in 1988 and joined the faculty of University of Illinois at Urbana-Champaign in 1991. He is the Eiszner Family Professor of Chemistry, and director of the Roy J. Carver Biotechnology Center; he is affiliated with the Institute of Genomic Biology and the Beckman Institute for Advanced Science and Technology. His research interests include the development of assays for complex microenvironments

including small-volume separation and detection methods, micro–nanofluidic sampling approaches and the application of these technologies to studying novel neurochemical pathways in a cell-specific manner. He is an associate editor of Analytical Chemistry.



Paul W. Bohn

Paul Bohn received his BS (University of Notre Dame, 1977) and his PhD (University of Wisconsin-Madison, 1981). After two years at Bell Laboratories in New Jersey, he joined the faculty at the University of Illinois at Urbana-Champaign. He is currently the Arthur J. Schmitt Professor of Chemical and Biomolecular Engineering at the University of Notre Dame. His research interests include: (a) studies of molecular transport on the nanoscale, (b) developing

optical spectroscopic measurement strategies for interfacial structure–function studies, (c) optoelectronic materials and devices and (d) molecular approaches to nanotechnology. Dr Bohn is the North American Associate Editor for Analyst.

current distribution and electroviscous effects in infinitely long cylindrical nanocapillaries. Their analysis starts from the Poisson–Boltzmann eqn,

$$\frac{1}{r} \frac{d}{dr} \left(r \frac{d\phi}{dr} \right) = \kappa^2 \phi, \quad (1)$$

where κ is the inverse Debye length given by

$$\kappa = \sqrt{\frac{8\pi n e^2}{\epsilon k T}}, \quad (2)$$

and the radial potential distribution in the capillary is given by

$$\phi = \phi_0 \frac{I_0(\kappa r)}{I_0(\kappa a)}, \quad (3)$$

where I_0 is the zero-order modified Bessel function of the first kind. For incompressible fluid under applied axial electric field, the equation of motion can be written as

$$\frac{1}{r} \frac{d}{dr} \left(r \frac{d\nu_z}{dr} \right) = \frac{1}{\eta} \frac{dp}{dz} - \frac{F_z}{\eta}. \quad (4)$$

Electro-osmotic velocity can be written as

$$\nu_z(r) = -\Omega E_z \left[1 - \frac{I_0(\kappa r)}{I_0(\kappa a)} \right]. \quad (5)$$

Several important implications follow from this work. There are two limiting cases, *cf.* Fig. 2. (a) $\kappa a \gg 1$ results in the classical case of electro-osmotic flow (EOF) with plug-like shape, observed in microfluidic experiments; (b) when $\kappa a \approx 1$, EOF is predicted to resemble Poiseuille type of flow, as has been verified experimentally.¹⁵ However this analysis gives only information about bulk fluid flow and does not consider transport of various species in solution.

Since then considerable efforts have been dedicated to further refine the understanding of transport in nanochannels, including refinement of continuum methods and molecular dynamics simulation of transport in small nanochannels and nanopores.^{16–18} A large body of work has been devoted to analyzing various nanofluidic elements (channels, conical pores, diodes, junctions, fluid networks) which are discussed in later sections of this paper.

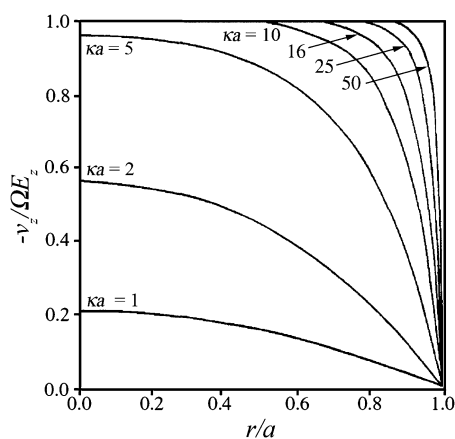


Fig. 2 EOF velocity profiles in infinite cylindrical capillary. Adapted with permission from ref. 14.

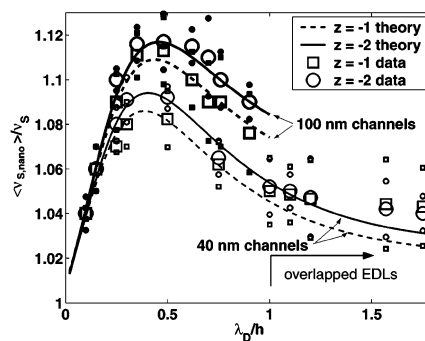


Fig. 3 Experimental and theoretical effective mobilities in nanochannels as a function of the EDL size. Reproduced with permission from ref. 19.

The condition $\kappa a \approx 1$ signifies that there is a significant interaction between two double layers, and most of the species are influenced by surface charge. In general transport rates across such nanofluidic features depend on a complex interplay of charge, electrophoretic mobility, molecule size (r_G), cross-section of a channel, ionic strength and surface charge. Flow rate normalized to cross-sectional area is less in nanochannels than in microchannels and limits translocation velocities. In addition to applied field, molecules are affected by the electric field due to the electrical double layer (EDL). As a result, counter-ions with larger charge are more attracted to the surface of the nanochannel and their migration is impeded most. Co-ions are repelled from edges of the channel and are transported faster than counter-ions. Neutral species are not significantly affected by the EDL and exhibit intermediate velocities (Fig. 3).^{16,19}

When molecular size approaches the size of a nanochannel, molecular transport is also affected by the space available for the molecule to explore in the nanochannel. Smaller molecules can approach closer to the channel walls than larger ones, and due to the Poiseuille-like flow profile that applies to nanochannels under $\kappa a \approx 1$ conditions, smaller molecules spend more time closer to the nanochannel walls and their translocation is slower than larger molecules that spend most of the time in the middle of the channel. Stein *et al.*²⁰ showed that this phenomenon, called Ogston sieving,²¹ is responsible for the dependence of DNA mobility in the nanochannel on the size of the molecule. In addition, macromolecules that are larger than the cross-section of the nanochannel undergo conformational changes, associated with an increase in entropy, upon entrance into confined space. Longer DNA strands move through such constrictions faster, because they have larger contact area at entrance and larger increase in entropy facilitates faster escape from the constriction. Han *et al.* have explored this principle for separations in nanofabricated sieving media.²²

Concentration polarization

In addition, transport in a nanochannel is affected by the nano–microfluidic junction region that can establish size or electrostatic exclusion, or concentration polarization, effects. Concentration polarization (CP) is based on the selective transport of counter-ions (relative to surface charge) through

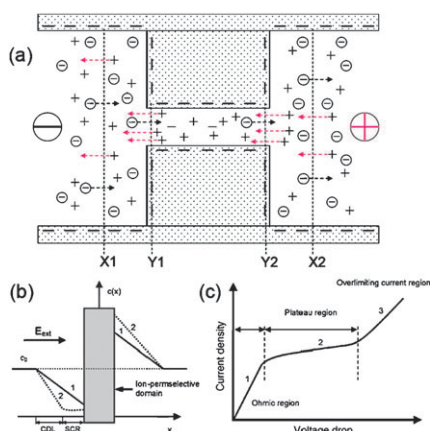


Fig. 4 Concentration polarization. (a) Schematic diagram illustrating the selective transport of cations through a nanochannel with negatively charged surface (adapted with permission from ref. 23); (b) concentration distribution during CP and (c) typical current across the nanochannel (adapted with permission from ref. 24).

nanofluidic channels filled with buffer exhibiting double-layer overlap. CP is a very general observation at nano–microfluidic junctions. Recently it has been reviewed and contrasted in nanofluidic channels, membranes, beds of mesoporous particles and monoliths.⁷ The mechanism giving rise to CP is illustrated schematically in Fig. 4. In the initial stage, Fig. 4(a), diffuse layers are formed at both nano–microfluidic junctions and the nanochannel is populated with counter-ions to the surface charge.²³

According to the current continuity constraint, the total charge coming through interface X1 is equal to that passing the smaller interface Y1. However, there are more cations than anions in the nanochannel due to the double-layer overlap; thus, more cations than anions pass interface Y1 from right to left, while an equal number of cations and anions pass interface X1 from left to right side. This selective transport of cations through the nanochannel results in the accumulation of both cations and anions in the bulk solution defined by the channel walls and interfaces X1 and Y1. On the anodic side of the nanochannel, a similar mechanism results in the depletion of both ions. Similarly, positively charged nanochannels selectively transport more anions than cations thus resulting in ion-enrichment on the anodic side and ion-depletion on the cathodic side.

Further increases in electric field magnitude result in an over-limiting electric current (stages 2 and 3 in Fig. 4(c))²⁴ which can be explained by the dynamic mechanism. The applied field induces the formation of a nonequilibrium double layer,²⁵ thus locally disrupting electroneutrality with extra cations, and causes nonequilibrium electro-osmotic slip.²⁶ This impulsive electro-osmotic flow brings ions forward across the diffusion limitation boundary, resulting in over-limiting current (cation transport) through the nanochannels. This process reciprocates to enable periodical fluctuations in the vicinity of the depletion region and through nanochannels.^{26–28} It is noteworthy that double-layer overlap is not a required condition to create the ion-depletion region, although it can accelerate the process of ion-depletion formation and exclude

co-ion transport thus inducing ion-enrichment on the other side of nanochannel.^{23,29,30}

3. Chemical analysis in nanochannels and nanopores

Nanofluidically enabled separations

Nanofluidics provide a good platform to investigate transport within well defined structures that can, in turn, lead to a better understanding of various separation mechanisms and development of new approaches for chemical separations.

Nanofluidic channels can be utilized to achieve chemical separations. In recent years intensive efforts have been dedicated to refine the theoretical description of separations in nanochannels. Griffiths and Nilson³¹ derived a relation for the dispersion in EOF flow for neutral species that in the thick EDL limit resembles Taylor dispersion observed in pressure driven flow. In subsequent work³² they theoretically analyzed separations of charged species in nanochannels. It was concluded that pressure driven separations discriminate based on species charge, while electrophoretic separations exploit a combination of charge and electrophoretic mobility. Xuan and Li reached similar conclusions³³ and proposed that optimal separations could be attained with a combination of pressure and electric field. Several theoretical studies have addressed the problem of ion dispersion in nanochannels.^{34–37} As illustrated in Fig. 5, two main factors affect ion dispersion: (a) interplay of flow profile and ion distribution in the channel, and (b) electrodispersion that limits diffusion due to electrostatic forces.³⁴ It has been shown that streaming potential generated during pressure driven separations reduces ion dispersion.^{35,38} In addition, rectangular channels display dispersion that depends on aspect ratio, more dispersion is expected in square channels than in rectangular ones.³⁷ Baldessari derived a formalism for electrokinetics in the overlapping EDL case and compared theoretical predictions with conductivity measurements.^{39,40}

There are fewer experimental studies on small molecule separations in nanochannels. Garcia *et al.*⁴¹ demonstrated separation of dye molecules in an array of nanochannels, following up with a demonstration that surface charge influences mobility of dye molecules in nanochannels.⁴² Pennathur and Santiago^{16,19} developed a model to describe

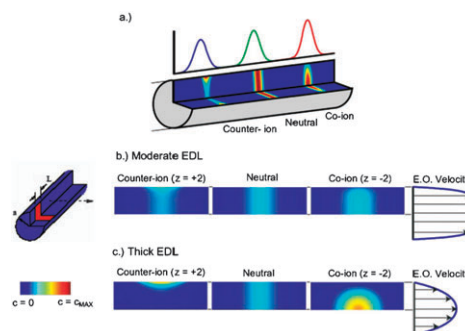


Fig. 5 Ion distribution in nanochannel supporting a separation. Reproduced with permission from ref. 34.

electrokinetics in nanochannels and used it to extract species charge from nanofluidic and microfluidic separations.

There has been considerable interest in using nanochannels to achieve improved separation of macromolecules. Macromolecule separation has been analyzed theoretically in slit-like nanochannels for both linear⁴³ and nonlinear⁴⁴ electromigration. According to this analysis resolution of macromolecules (with a size less than the nanochannel) is significantly increased due to interactions with the walls. Separation of short dsDNA (< 100 bp) was demonstrated in a nanochannel.⁴⁵ However most of the emphasis has been on the design and utilization of well defined nanofabricated materials. Three particular examples deserve special mention. Han and Craighead demonstrated separations in nanostructures exhibiting alternating deep and shallow regions^{46,47} by exploiting different DNA translocation speeds across shallow regions. Separations based on both entropic trapping⁴⁷ and Ogston sieving⁴⁸ were shown. Recently 2D sieving media have been fabricated and continuous separation demonstrated.^{49,50} These efforts have been reviewed recently.^{12,22}

Well defined nanostructures for nanoscale separations can also be created by self-assembly of colloidal particles. DNA migration in self-assembled nanosphere beds leads to a larger range of mobilities and to improved separations for short (< 1000 bp) DNA strands.^{51,52} Well defined nanopillars have been utilized as a sieving medium for long strand (1 to 100 kbp) DNA separations. Nanopillars can be defined using e-beam,⁵³ nanoimprint⁵⁴ or nanosphere⁵⁵ lithography. Nanopillar formation by nanosphere lithography is especially attractive due to the simple fabrication process and tunability of nanopillar size.

Microsensors

The large surface–volume ratio and small cross-sectional size of nanochannels make diffusion a viable mode of transport from bulk solution to the surface, thereby facilitating surface processes such as sensing or affinity preconcentration. Efforts have been made to modify inner nanochannel surfaces with molecular recognition agents such as antibodies and DNAzymes.^{56–58} Lee *et al.* reported an antibody-based biosensor for enantiomer recognition and separation in 2002.⁵⁹ Alumina nanopore films were used and silica nanotubes were deposited into the alumina nanopores to achieve pore diameters of 20–35 nm; then aldehyde reactive groups were attached to the silica nanopores by reacting silica hydroxyl groups with an appropriately chosen silane; finally, antibody molecules were anchored to aldehyde groups by chemical reaction with amino groups. The authors demonstrated the selective transport of the enantiomer that specifically bound to the antibody while the other enantiomer was rejected. Wernette *et al.* developed a Pb²⁺ sensor by using fluorescently labelled DNAzyme as the signalling agent.⁵⁷ A polycarbonate nanocapillary array membrane (NCAM) was first coated with gold using electroless plating,^{60,61} then thiolated DNAzyme was tethered to the gold-coated nanopore surface, and finally a fluorescently labelled substrate strand was hybridized to the immobilized enzyme strand. When Pb²⁺ contacted the enzyme, the substrate chain was cleaved and fluorescence

was detected in solution. In this Pb²⁺ sensor, nanopores provide a large surface-to-volume ratio, so that signal intensity is enhanced. Subsequently, Kim *et al.* directly immobilized Fab' in nanopores of an NCAM to specifically capture and release target molecules.⁶² Electroless deposition of Au in nanopores of an NCAM and thiol-gold chemistry were used to realize the molecular recognition motif in the nanoflow format. Then offline MALDI-TOF mass spectrometry was used to confirm the identity of the collected and released components. Further efforts have demonstrated how to integrate Au-functionalized NCAMs with microfluidics. Piruska *et al.* studied electrokinetic fluid transport property through gold-coated nanopores in an NCAM⁶³ and concluded that, despite their large conductance, gold-coated nanopores could support electrokinetic injection under well defined conditions of current path and electric field distribution, while avoiding bubble formation due to electrolysis. This research demonstrates the possibility of integrating molecularly-functionalized NCAM-microfluidics for mass-limited chemical analysis.

Resistive-pulse sensing

A nanochannel (or a nanopore) can serve as a sensor for molecules that approach the cross-sectional size of the channel.

Translocation of large molecules through nanopores induces a transient nanopore blockage which produces a decrease in current.^{64–68} This current change can be used to count and size molecules. The principle is equivalent to that used in Coulter counting, a commercially available device capable of counting and sizing biomolecules and particles.⁶⁶ In 1994, Bezrukov *et al.* reported counting polyethylene glycol (PEG) molecules passing through single nanochannels formed by natural pore-forming peptides in a bilayer lipid membrane, demonstrating the capability to detect single molecules with a radius of gyration as small as 0.5–1.5 nm.⁶⁹ Starting with two ionic solutions on each side of the nanopore, a voltage is applied, electrokinetically driving charged molecules through the nanopore. Because the size of the molecules, *e.g.* DNA, is

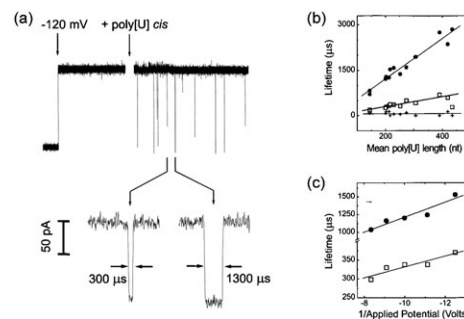


Fig. 6 (a) Single poly[U] molecules cause transient blockades of α -hemolysin single channels thus inducing an ionic current decrease with different lifetimes as shown in the insert (expanded view). The translocation time of single poly[U] molecules is proportional to (b) the polymer length and (c) inversely proportional to the applied voltage. The plots show lifetimes for (a) peaks 1 (+), 2 (□) and 3 (●) in experiments using $V = -120$ mV with 13 different size selected poly[U]s and (b) for peaks 2 (□) and 3 (●) with poly[U] of mean length 215 nt at the indicated voltages. Adapted with permission from ref. 65.

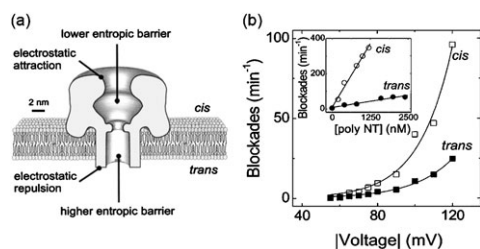


Fig. 7 (a) Schematic structure of an α -hemolysin nanopore embedded in a lipid bilayer. The *cis* side has a larger opening with lower entropic barrier while the *trans* side has a smaller opening with higher entropic barrier. (b) Voltage and concentration dependence of the rate of blocking the current by a polynucleotide. Adapted with permission from ref. 68.

comparable to the nanopore diameter, other ions are repelled from the nanopore pathway temporarily, resulting in the observed current decrease (Fig. 6). A number of different ion channels have been used for DNA or RNA translocation experiments,^{65,70,71} however by far most popular is α -hemolysin due to its well studied structure, stability, ability to introduce various modifications. α -Hemolysin is a 293-amino acid protein secreted by *Staphylococcus aureus*.⁷² Seven α -hemolysin monomers form heptamer nanopores through self-assembly and are embedded across a lipid bilayer.⁷² The size of a formed nanopore is in the range of 1.5–2.6 nm, just the right size to allow passage of single-stranded DNA or RNA molecules.

Careful quantitative studies have shown that the translocation time of polynucleotides (*i.e.* residence time in nanochannels) is proportional to the polymer length and inversely proportional to the applied voltage, Fig. 6(b). Therefore, the length of polymers can be determined from their nanopore translocation times. Moreover, as shown in Fig. 7, the chain components and structure affect the nanochannel blockage extent and translocation duration.^{73–75} The passage of each ssDNA or RNA molecule induces a transient ionic current decrease with a duration proportional to its individual length.⁷⁶ This can be used to determine the length of polypeptides and their identities, and potentially provides a fast method for sequencing DNA or RNA bases.^{77–79} In 1996, Kasianowicz *et al.* characterized individual polynucleotides using a nanochannel in a lipid bilayer with 2.6 nm channel diameter.⁶⁵ In 2000, Meller *et al.* demonstrated rapid discrimination of single polynucleotides with α -hemolysin nanopores,⁷⁰ showing the capacity to distinguish polynucleotides with similar length and composition differing only in sequence. They also demonstrated that the translocation duration was temperature dependent as T^{-2} . In 2005, the Meller group reported that the passage of single-stranded DNA through an α -hemolysin nanochannel discriminated orientation in favor of 3'-threaded DNA by 30% more than 5'-threaded.^{71,80} It also provides a way to investigate molecular recognition interactions in nanopores.⁸¹

Kasianowicz *et al.*⁸² demonstrated that single nanopore translocation can resolve different PEG homologs. They showed that polymer mass distribution can be obtained by deconvoluting the duration of translocation using a Gaussian mixture model, as shown in Fig. 8.

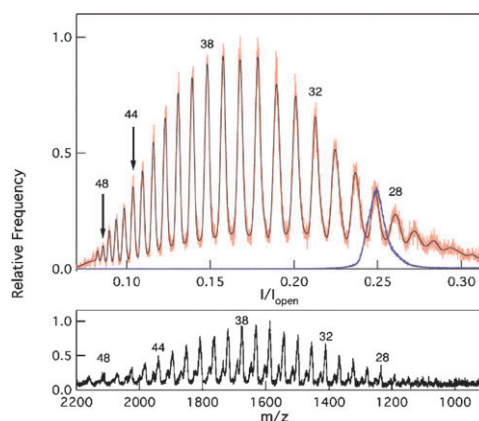


Fig. 8 Comparison of the histogram of translocation duration through α -hemolysin nanopore and MALDI TOF mass spectrum of PEG homologs. Adapted with permission from ref. 82.

Recent efforts in resistive-pulse sensing have focused on artificial solid-state nanopores.^{83,84} In 2001, Li *et al.* developed “ion-beam sculpting” to fabricate dimensionally-controlled nanoscale holes in thin solid-state membranes⁸⁴ and demonstrated the capability of detecting single DNA molecules with nanopores in Si_3N_4 . In 2003, Saleh and Sohn used micro-molding to fabricate nanoscale pores in PDMS, thereby developing a platform offering flexibility and convenience for single DNA molecule detection.⁸⁵ Folega *et al.* demonstrated that translocation events occur over a distribution of folded and unfolded configurations.⁸⁶ Gershow and Golovchenko investigated the mechanism and dynamics of recapturing and trapping single DNA molecules in a solid-state SiN nanopore as shown in Fig. 9.⁶⁴ Wanunu *et al.* investigated the voltage-driven translocation dynamics of single DNA molecules through solid-state nanopores and concluded that DNA translocation is governed by the interactions of DNA molecules with the nanopore wall.⁸⁷ Finally resistive-pulse sensing has also been applied to detecting single protein molecules, since the size of large protein molecules is comparable to nanofabricated pores. Han *et al.* first reported the detection

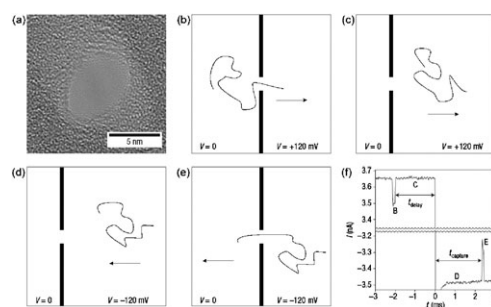


Fig. 9 (a) Transmission electron microscopy image of the SiN nanopore. (b–e) Schematic sequences of the translocation and recapture process. Arrows indicate the DNA migration direction and the electric force direction; a single DNA molecule passed through the nanopore and kept migrating forward under the influence of the electric field and then migrated backward and finally passed through the same nanopore in the reversed direction. (f) A typical current signal track with normal and reversed voltage applied across the nanopore membrane; the letters indicate the corresponding current in sequences shown in (b–e). Reproduced with permission from ref. 64.

of single BSA protein molecules with nanofabricated nanopores based on repulsive sensing method in 2006.⁸⁸

Early on, workers realized that adding either chemical or geometric asymmetry to nanopores could lead to interesting physical properties. Pioneering work with conical nanopores was initiated by Martin and co-workers.⁸⁹ Conical nanopores were first fabricated by track-etching, in which a polymer membrane was first bombarded with high-energy particles, and then the damage track was etched in base, while neutralizing the incoming basic solution from the other side to form cylindrical pores.⁹⁰ Conical nanopores have some distinct advantages over conventional cylindrical pores in resistive-pulse sensing, including being more sensitive due to ionic current focusing at the conical tip, exhibiting larger ion currents at equivalent diameters, and being more resistant to fouling. Two types of sensors have been developed employing conical nanopores: resistive-pulse sensing and specific molecular recognition nanopores modified with ligands.^{58,91,92}

Heins *et al.* demonstrated the first detection of a single abiotic molecule using resistive-pulse sensing method with a single conical nanopore⁹¹ utilizing a membrane with conical nanopore diameter of ~ 4.5 nm, comparable to the diameter of the target porphyrin. Conical sensing elements have also been tested for the detection of single-stranded DNAs using a tip diameter of 40 nm.⁹² Electrical current measurements showed that the ssDNA can translocate through and produces smaller current variation and shorter translocation time compared to dsDNAs, as shown in Fig. 10. Therefore, the conical nanopore is capable of discriminating ssDNA from dsDNA.

The utility of size-restrictive nanopores can be significantly extended by adding molecular recognition motifs to the interior of the nanopore. Martin and co-workers developed an efficient method based on electroless deposition of a thin gold layer on the interior surface of the polymer nanopore.^{58,60,61,93–98} This, in turn, provides wide range of possibilities for nanopore modification using well established Au-thiol self-assembly chemistry.

Siwy *et al.* fabricated protein biosensors by using surface biofunctionalized nanotubes.⁵⁸ They first plated a thin layer of gold into the conical nanopores as well as both faces of

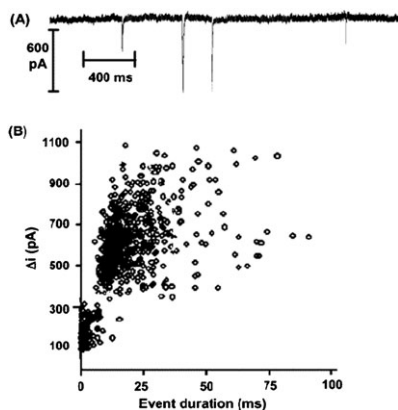


Fig. 10 (a) Current–blockage events for a mixture of dsDNA and ssDNA. (b) Scatter plot showing magnitude of current variation (Δi) vs. blockage duration for the ssDNA and dsDNA mixture. Adapted with permission from ref. 92.

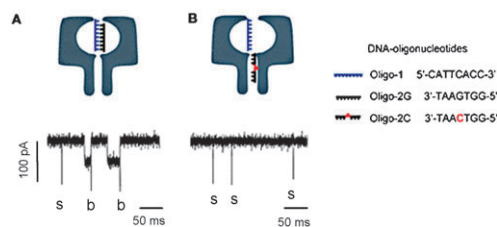


Fig. 11 Schematic diagram showing duplex formation event (A) and single-base mismatch abolishes the binding (B) of an oligonucleotide to a tethered DNA strand within a DNA-nanopore. The short spike (s) in the current trace is a translocation event of Oligo-2G that did not bind to the tethered Oligo-1; the binding event (b) causes a shorter and wider current variation followed by a translocation process after dissociation. Adapted with permission from ref. 99.

membrane by electroless deposition,⁶⁰ then thiolated biotin derivatives were attached to the gold surface by self-assembly. The authors tested the performance of the biosensor for streptavidin detection by relating blockage time to streptavidin concentration. The biosensor was further modified by attaching biotinylated protein G for IgG recognition through a biotinylated streptavidin linker which was immobilized to the anchored biotin, thereby achieving a versatile molecular recognition platform that could be melded to a variety of different surface chemistries.

Nanopores have also been engineered with DNA strands to form DNA nanopores, by covalently attaching ssDNA to the α -hemolysin nanopores.⁹⁹ One of the seven α -hemolysin oligomers is modified with a single oligonucleotide, *e.g.* Oligo-1 (5'-CATTACC-3'). When a sequence, *e.g.* Oligo-2G (3'-GTAAGTAA-5') complementary to the tethered Oligo-1, is added to the *cis* side, Oligo-2G first binds to form a DNA duplex, thus causing a current decrease with a characteristic time duration. When the complex finally dissociates and passes through the pore, a current transient results from the momentary blockage of the inner constriction bottle neck, as shown in Fig. 11(A). On other hand, a sequence (Oligo-2C, 3'-TAACTGG-5') with only one base mismatch has no chance to form a duplex with Oligo-1 and directly passes through the nanopore inducing only narrow current spike with a typical duration of ~ 0.15 ms as shown in Fig. 11(B). Moreover, even the entrance direction of Oligo-2G is critical to duplex formation, so that entrance of the 5' end from the *cis* side results in no binding events. Finally, Purnell *et al.* modified ssDNA by attaching a streptavidin to biotinylated ssDNA and demonstrated orientation discrimination of ssDNA at α -hemolysin nanopores.¹⁰⁰ The immobilization of ssDNA to nanopores is based on the fact that the streptavidin is too large to fit either part of the nanopore and stays outside of the pore while serving as an anchor to tether ssDNA when a voltage is applied across the nanopore. Most recently, Stoddart *et al.* employed this strategy to discriminate among single nucleotides by current measurements.¹⁰¹

Fluidic circuits—diodes, transistors

It has been pointed out that ions in nanochannels have qualitative similarities to charge carriers in semiconductors.¹⁰²

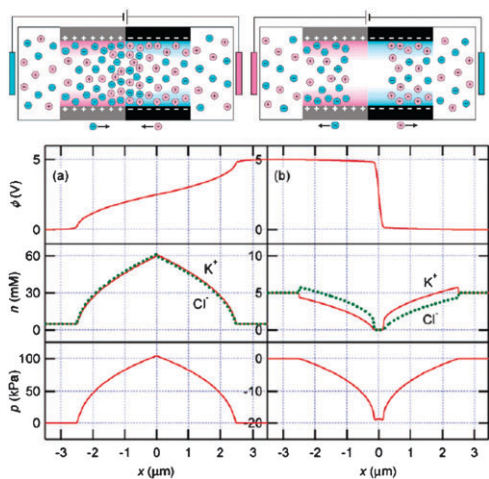


Fig. 12 Ionic concentrations in nanofluidic diode during forward (a, left) and reverse (b, right) bias. Reproduced with permission from ref. 107.

One can imagine that by manipulating surface charge density control of ionic species in nanochannels can be achieved.

The most studied fluidic analog to semiconductor component is a diode.¹⁰² Similarly to their semiconductor counterparts, fluidic diodes exhibit current rectification depending on the polarity of the applied bias. Current rectification is achieved by breaking the symmetry of the nanochannel, by changing the cross-section along the nanochannel length, controlling electrolyte concentration in adjacent reservoirs or modifying the spatial distribution of charge density within the nanochannel. Geometric variations in cross-section are often intrinsic to nanopore construction techniques. However, a more elegant and useful method to achieve directional anisotropy for chemical analysis is surface charge modification. Various types of nanofluidic diodes have been analyzed,^{103–106} and the strongest current rectification is achieved in nanofluidic channels with abrupt changes in surface charge polarity (Fig. 12).¹⁰⁷ Theoretical modelling shows that during forward bias both cationic and anionic concentrations increase at the surface charge discontinuity, while there is a very strong depletion of both types of ions during reversed bias. Recently, pH dependent diodes^{108,109} and diodes with tuneable¹¹⁰ current rectification were demonstrated, and the degree of current rectification can be used for biosensing.¹¹¹

Karnik *et al.* demonstrated nanofluidic field effect transistor where gate electrodes control surface charge, and consequentially ionic concentration and conductance, in a nanochannel.¹¹² Control over protein transport was demonstrated in a device with two nanofluidic transistors.¹¹³ Daiguji *et al.*¹¹⁴ extended this concept by theoretically analyzing nanochannel junction structures analogous to *pn*p transistor. Their analysis revealed that ionic current can be regulated and manipulated in such junction(s). Recently, such structures have been demonstrated experimentally by Cheng and Guo.¹¹⁵ They fabricated *pn* and *pn*p diodes and triodes utilizing alumina features in silica. This presents opportunities to fabricate more sophisticated fluidic circuits for analysis/separation of ionic species. At present, only individual fluidic components have been studied, however it is reasonable to expect further refinement of individual components

and attempts to create more sophisticated fluidic circuits for chemical/biochemical analysis.

Single molecule manipulations

Optical detection, especially laser-induced fluorescence (LIF) detection, prevails in current single molecule analysis, and when combined with nanofluidics there are distinct advantages for single molecule detection. In a typical confocal single molecule fluorescence correlation spectroscopy experiment, the excitation volume is determined by diffraction limited focused beam size, which is of order of 0.2 fL. In order to observe single molecule events, the fluorophore has to be kept at nanomolar and lower concentration, thus naturally limiting the range of K_D values for binding reactions that can be studied.¹¹⁶ Nanochannels (or pores) can, by the simple fact of presenting a smaller experimental volume, provide larger confinement, thus allowing experiments to be performed at higher concentrations.¹¹⁷ Confinement can be achieved either by a planar nanochannel or using zero mode waveguide (ZMW), nanopore or nanopit in substrate covered with metal layer.

Large biomolecules, including DNA and proteins, are typically the targets of single molecule manipulations, including separation, sequencing, and biophysical measurements, among which single DNA confinement and linearization are the most widely studied phenomena.¹¹ DNA comprises various numbers of nucleotides interconnected by phosphate ester bonds with ~ 2 nm diameter, 0.34 nm linear distance per nucleotide base pair, but up to a centimetre total physical length. Double-stranded DNAs (dsDNAs) are stiff worm-like chains with complex conformational structural behaviors, such as folding, twisting, and supercoiling.¹¹ Commonly, genetic information is sought from DNA, and physical gene mapping by restriction or molecular combing is required to locate gene positions.^{118,119} Nanochannels offer an ability to confine DNA molecules linearly and manipulate long DNA precisely, which provides a powerful tool for studying DNA mechanical and physical properties.^{4,11}

ZMWs, *viz.* Fig. 13, allow excitation volumes as low as zL^{116} (10^{-21} L, ~ 4 orders of magnitude lower than obtainable with diffraction limited techniques) which translates into the ability to interrogate single molecules at concentrations of $\sim 200 \mu\text{M}$. In turn this is very advantageous for studies of binding events of enzymes at physiologically relevant concentrations.¹²⁰ Thus, ZMWs were initially combined with biological systems to allow study of single binding/catalysis events for systems with μM ligand concentrations.^{116,121–123} Consisting of

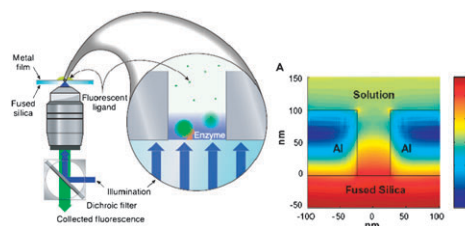


Fig. 13 Experimental schematic for ZMW optical excitation (left), simulated electric field distribution in ZMW (right). Reproduced with permission from ref. 116.

zeptolitre volume cylindrical (typically $d = 50\text{--}100$ nm and thickness = $60\text{--}100$ nm) nanopores in an opaque film (typically Al^{124,125}), ZMWs serve to enhance the amplitude of the electromagnetic field and thereby the signal inside the nanocylinder relative to the background in linear spectroscopic experiments. Furthermore, because the light propagation is strongly damped in the far-field of the ZMW, there is little stray field amplitude to give rise to spurious background signals from solution outside the ZMW volume. Thus, owing to their small volume, excellent optical confinement and signal enhancement, and spatial localization, ZMWs are increasingly of interest in studies of biological chemistry, ranging from DNA sequencing of single polymerase molecules¹²⁶ to protein–protein interactions¹²⁷ to studies of plasma membrane dynamics.^{121,123,128} Furthermore, the spectroscopy can be accomplished either in imaging mode, in which a large number of parallel ZMWs can be interrogated simultaneously,^{124,125,127} or by FCS.^{121–123,128}

4. Chemical analysis in nanofluidic–microfluidic hybrid structures

Sample concentration

To conveniently handle mass-limited samples, a minimum sample volume is required even when analyzed on microfluidic devices capable of manipulating tiny sample volumes. If the number of analyte molecules distributed in the sample volume is small enough, extremely dilute solutions may be obtained that pose especially difficult challenges for detection. Therefore, sample preconcentration prior to measurement is strongly advantageous when the limit of detection (LOD) is insufficient for specific applications. Traditional electrophoretic sample concentration methods, such as sample stacking,¹²⁹ sweeping,^{130–132} and solid phase extraction,^{133,134} can have issues when used with microfluidic devices. Therefore, nanofluidic components have been integrated into microfluidic devices for sample concentration. Nanofluidic channels, due to the propensity for concentration polarization, exhibit ion permselective transport capability.¹³⁵ There are a number of distinctive features of the nanofluidically induced sample concentration effect: (i) ion permselective transport causes ion-enrichment; (ii) nanofilters prevent large molecules from passing, providing an intrinsic size selection; and (iii) electric field-induced double layers repel charged analytes. Prior to the development of a full understanding anion-enrichment behavior was ascribed to nanochannels.^{136,137} The coupled effects just listed were appreciated once it was understood that current continuity is established only after a bias is applied across the hybrid micro–nanochannel for a period of time, thus discharging the nanochannel capacitance, as investigated by Chatterjee *et al.*¹³⁸

Utilizing CP Han *et al.* obtained a million-fold preconcentration of proteins at a nanofluidic–microfluidic junction.²⁹ It is interesting to note that the enriched protein plug was observed on the anodic side of the nanochannel instead of the cathodic side where it would be expected for a negatively charged nanochannel. The same preconcentration mechanism can be employed in devices prepared using simpler

fabrication methods. For example, Lee *et al.* developed a nano-gap breakdown method to obtain 10^4 -fold concentration of specific proteins in an hour.¹³⁹ The nanochannels were fabricated by applying a high voltage (1000 V) across two individual microchannels with a close parallel point to induce nano-gap breakdown. Obviously, this nano-gap breakdown is less controllable than lithographically prepared structures, since many factors affect the mechanic characteristics of PDMS, such as the ratio of PDMS prepolymer and curing reagent, curing time and temperature, buffer concentration, and magnitude of the applied voltage. To improve the nano-gap fabrication, Lee *et al.* utilized ion-selective polymer membrane to serve as the nano conduits interconnecting microfluidic channels.¹⁴⁰ Nafion, a sulfonated polymer based on tetrafluoroethylene, is able to selectively transport cations. A thin layer of nafion was coated on a piece of cover glass by microcontact printing or microflow patterning.¹⁴⁰ The authors used this device to investigate low-abundance enzyme kinetics after concentrating enzyme and substrate in the same plug and significantly enhanced the reaction rate and detection sensitivity.

Protein preconcentration based on size exclusion has also been demonstrated using nanofluidic components coupled to microfluidics.^{141,142} Proteins are relatively large molecules and are hindered and accumulated by the molecular weight cutoff characteristic of nanochannels. Song *et al.* fabricated a nanoporous membrane at the junction of microfluidic channels by using laser-patterning.^{141,143} The polymer nanoporous membrane served as a nanofilter to concentrate proteins with molecular weight above 5700 Da, while buffer ions could easily pass through the nanofilter. Up to 4 orders of concentration enhancements were obtained in 100 s under a moderate voltage. Foote *et al.* reported a similar microfluidic device coupled with a porous silicate-bonding layer fabricated using standard wet-etching.¹⁴² Similarly, the nanoporous layer allowed the passage of buffer ions, while it retained and concentrated protein molecules with up to 600-fold signal enhancements after SDS-CGE separation. Both methods use electrophoresis to bring negatively charged proteins to the concentrated plug on the cathodic side of the nanoporous membrane where ion-enrichment may occur. Under an applied voltage across a nano/microfluidic interface, proteins are electrokinetically transported and serve as current carriers together with buffer ions. On the one hand, large protein molecules are restrained and accumulate at the interface of the microchannel and nanochannel. In addition, negatively charged nanochannels with EDL overlap are able to exclude co-ions, including proteins with low pI values, and selectively allow counter-ions to pass.¹⁴⁴ Therefore, the ion-enrichment capability of nanochannels may work synergistically with size selection in protein concentration strategies employing nanofluidic filtration.

For example, Kim *et al.* demonstrated a simple PDMS–glass microchip for electrokinetic protein concentration on the anodic side of the nanocomponents.¹⁴⁵ The microchannels were fabricated in PDMS and then covered with glass by a weak and reversible bonding method. The authors hypothesized that a spontaneous nanochannel was formed between glass and PDMS and confirmed this hypothesis using permanent

bonding to eliminate protein concentration until the PDMS was subjected to electrical breakdown in a high electric field. They achieved up to 10^6 -fold preconcentration in 30 min.

Nanofluidically enabled sample preconcentration in microfluidic structures has attracted great attention. The mechanism of ion-depletion and enrichment has been extensively studied, but a number of important details remain poorly understood. For example, the nonequilibrium double layer induced by applied electric field was postulated to be the key factor that accounts for sample concentration.²⁹ However, further studies should include the mass transfer rate through nanochannels, electric field distribution across the microfluidic channel, filling with different-conductivity buffers (after ion-depletion), and balance of forces between electrophoresis and electroosmosis.

Nanofluidic injection

Nanochannels can also be used as fluidic interconnects between vertically separated microfluidic channels to achieve 3D integrated microfluidic architectures. Fluid flow can be electrokinetically switched on and off to execute sample introduction from the sample source microchannel to the downstream receiving microchannel. The details of the mass transport can be controlled by appropriate combinations of nanochannel surface charge and diameter, buffer pH and ionic strength, and analyte properties.¹³⁵ In particular, transport conditions can be adjusted by the relative magnitudes of nanochannel diameter, a , and double layer thickness (κ^{-1} , *i.e.* Debye length). When $a \approx \kappa^{-1}$, EDL overlap occurs, thus facilitating selective transport of counter-ions over co-ions. If the magnitude of electroosmosis in the nanochannels is larger than that of analyte electrophoresis and in the opposite direction, co-ions can still be swept across the

nanochannels.¹³⁵ When $a \gg \kappa^{-1}$, nanochannel surface properties and buffer pH interact to resolve how the combination of electroosmosis and electrophoresis add to analyte transport direction as shown in Fig. 14.^{137,146} When $a > \kappa^{-1}$ by relatively small factors (10- to 100-fold), nanochannels still selectively transport counter-ions.²⁹ Note that Debye length is usually in the range of 1 to 10 nm and is adjustable by varying buffer ionic strength.

Recently, King *et al.* investigated the electrokinetic transport properties of polyelectrolytes (polystyrene sulfonate, polyallylamine, and DNA) through a single nanopore.¹⁴⁷ The nanopores with a diameter of 180 nm were fabricated in PMMA membranes using focused ion beam milling, and then a single nanopore was sandwiched between two crossed microfluidic channels. Both electrical current measurements and confocal fluorescence imaging showed that electroosmosis through the nanopore predominates over electrophoresis in the transport of polyelectrolytes, because of the 180 nm pore where $a \gg \kappa^{-1}$; moreover, $\zeta < 0$, so the negatively charged nanopore surface demonstrates strong permselective transport property in favor of cationic polyelectrolytes (polyallylamine) over anionic species (polystyrene sulfonate).

Electric field extension through nanopores has also been used to obtain less expanded sample plugs.^{148,149} A voltage is applied across the injection, *i.e.* source, channel, and an electric field extends through the nanopores to the cross-section of the separation, *i.e.* receiving, channel, thus electrokinetically driving charged analytes through the nanopores. The injected analytes accumulate in the cross-section, since the electric field in the cross-section of the separation channel is perpendicular to the channel. Therefore, improved separation efficiency and signals are achieved.

Nanovalves

Integrated NCAMs between microfluidic channels can maintain separate environments, as demonstrated by profiling pH gradients across an NCAM.¹⁵⁰ Two fluorescent solutions at different pH values ($\Delta\text{pH} \approx 3.0$) were loaded into two separate microfluidic channels interconnected with an NCAM containing 10 nm diameter nanopores. The fluorescence intensity did not change after 120 min at steady state, establishing that 10 nm NCAMs are able to maintain separate operating conditions with high fidelity, while 200 nm diameter NCAMs were much less effective.

Single nanofluidic channels or nanopore arrays sandwiched between microfluidic channels can serve as interconnection conduits and nanovalves for selective sample injection and plug collection after electrophoretic separation. When no field is applied, molecular diffusion dominates, as expected in hydrophilic nanochannels, *e.g.* polyvinylpyrrolidone (PVP)-coated polycarbonate (PC).¹³⁵ However, diffusion becomes negligible when hydrophobic nanochannels, *e.g.* uncoated PC, are used.¹³⁵ Therefore, nanocapillary array membranes have been integrated between microfluidic channels to serve as nanovalves during electrokinetic transport and electrophoretic separation.^{56,135,149} In the presence of applied fields, the digital fluidic switching properties of NCAMs dominate, allowing a wide variety of useful fluidic manipulations to be realized.

For example, a second molecular gate can be integrated downstream along the microfluidic separation channel for specific

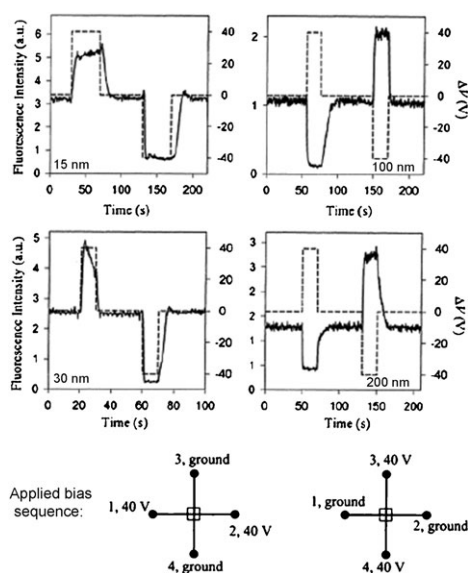


Fig. 14 Electrical bias activated reagent transport through nanochannels. Fluorescence intensity (left ordinate, solid line) vs. applied bias ΔV ($V_{\text{receive}} - V_{\text{source}}$, right ordinate, dashed line), as a function of time in the receiving microchannel (1–2) showing transport of 0.17 μM fluorescein in 5 mM pH 8 phosphate across polycarbonate NCAMs with various pore diameters as shown in figure block. Adapted with permission from ref. 137.

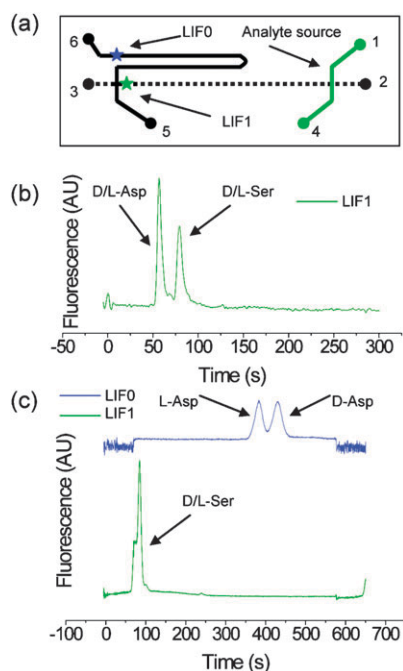


Fig. 15 (a) Channel layout of the hybrid micro–nanofluidic device. An NCAM with 220 nm diameter pores is sandwiched between dashed and solid channels. Stars indicate the laser-induced fluorescence detection points. LIF1 monitors the first-stage separation channel close to the cross-section as indicated and is used to indicate specific peak collection; and LIF0 monitors second-stage separations. (b) First-dimensional separation of a racemic mixture containing FITC-labelled aspartic acid (D/L) and serine (D/L) without enantiomer resolution. (c) The sequential two-stage separations of FITC-Asp and FITC-Ser, where the FITC-Asp (D/L) is selectively collected in the second-stage separation channel for the chiral separation. Adapted with permission from ref. 56.

sample plug collection and for second-stage separation.^{56,151} As shown in Fig. 15, a sample plug separated into individual components can be selectively collected at the second NCAM gate¹⁵¹ and further processed in secondary microchannel. Recently, Kim *et al.* utilized this capability to perform multiple-stage chiral separations in a hybrid micro–nanofluidic device coupled with molecular gates at both sides of the first-stage separation channel as shown in Fig. 15.⁵⁶ A sample plug injected through an NCAM molecular gate on the right side was electrophoretically separated by the first-stage separation channel. Then a specific band was collected through the NCAM and subjected to second-stage separation containing a chiral selector in the running buffer. The NCAM on the one hand serves as sample injector and valve during the first-state separation so that no pushback voltage is applied to the analyte source channel; on the other hand, the NCAM on the collection side is able to keep two buffer systems from mixing while simultaneously being able to collect sample through the nanopores. Therefore, NCAM-coupled microfluidic devices provide a convenient platform for complex multi-dimensional chemical analysis.

Nanofluidically enabled micromixer

Microfluidics allows ultra small sample volumes to be manipulated, thus providing a practical platform for handling mass-limited samples. However, the small Reynolds numbers

characteristic of microfluidic flow lead to laminar flow, instead of vortices, eddies, or other random fluctuations present in turbulent flow at larger Reynolds numbers. Therefore, mixing in microfluidic systems originates from diffusion and is, consequently, slow, unless aided by extraneous fluidic mixing elements, such as zigzag microchannels,^{152–154} vortex chambers,¹⁵⁵ or strategies to produce forced mixing using chaotic electric field, ultrasonic vibration, and magnetic forces.^{156–158} Alternatively, nanochannels offer a rapid mixing approach based on convective flow from nanochannels to the microchannel.¹⁵⁹ Fast diffusive mixing in the lateral direction was expected due to the small pore-to-pore separations. However, rapid mixing was also observed in the vertical dimension, later determined to be caused by the accumulation/depletion effects at the micro–nano boundary discussed above, establishing an electro-osmotic flow of the second kind and corresponding convective vortices.¹⁶⁰

5. Conclusions

Nanofluidic architectures have proven to be a nearly ideal complement to microfluidic networks for applications in chemical analysis. In this review, we have examined the major drivers for nanoscience in the context of chemical analysis applications: new phenomena at the nanoscale (Poiseuille-like flow, nanovalving, nanoinjections); large surface-to-volume ratio (nanoscale affinity/molecular recognition); diffusion as a viable mechanism for mass transport (diffusive mixing for fast kinetics); and the size commensurate nature of nanopores and molecular constructs (resistive-pulse sequencing). Clearly, the extended capabilities provided by the integration of nanofluidic elements within more traditional microfluidic architectures expand the ability to perform complex analytical operations on mass-limited samples while retaining sample integrity, and the explosive growth of work in this fruitful area shows no signs of slowing.

While the theory, design and creation of fluidic elements on the nanoscale is a relatively new area of biophysics/bioengineering/analytical chemistry, biologists have been studying molecular transport through channels for decades. As our understanding of the unique characteristics available in this size regime increases, our ability to (re)create pores with the exquisite functionality of biological proteins in membranes may finally become a reality. By creating such tailored nanofluidic elements, will we add a suite of physically responsive channels, selective single molecule detectors based on engineered pore proteins, artificial enzymes with a reactivity dictated by the nanochannel shape, and devices with hybrid electronic/fluidic/enzymatic elements to the lab-on-a-chip devices of the future.

Acknowledgements

The material presented here from the authors' laboratories was supported by the National Science Foundation under Award No. DMI-0328162 (NanoCEMMS) and cooperative agreement CTS-0120978 (Water CAMPWS), the Department of Energy DE FG02 07ER15851 and the Strategic Environmental Research and Development Program under Award No. W9132T-05-2-0028.

References

- 1 A. Manz, N. Graber and H. M. Widmer, *Sens. Actuators, B*, 1990, **1**, 244.
- 2 R. B. Schoch and P. Renaud, *Appl. Phys. Lett.*, 2005, **86**, 253111.
- 3 D. Mijatovic, J. C. T. Eijkel and A. van den Berg, *Lab Chip*, 2005, **5**, 492.
- 4 P. Abgrall and N. T. Nguyen, *Anal. Chem.*, 2008, **80**, 2326.
- 5 R. B. Schoch, J. Han and P. Renaud, *Rev. Mod. Phys.*, 2008, **80**, 839.
- 6 M. Rauscher and S. Dietrich, *Annu. Rev. Mater. Res.*, 2008, **38**, 143.
- 7 A. Hölzel and U. Tallarek, *J. Sep. Sci.*, 2007, **30**, 1398.
- 8 Z. Yuan, A. L. Garcia, G. P. Lopez and D. N. Petsev, *Electrophoresis*, 2007, **28**, 595.
- 9 P. W. Bohn, *Annu. Rev. Anal. Chem.*, 2009, **2**, 279.
- 10 J. O. Tegenfeldt, C. Prinz, C. Han, R. L. Huang, R. H. Austin, S. Y. Chou, E. C. Cox and J. C. Sturm, *Anal. Bioanal. Chem.*, 2004, **378**, 1678.
- 11 N. Douville, D. Huh and S. Takayama, *Anal. Bioanal. Chem.*, 2008, **391**, 2395.
- 12 J. Fu, P. Mao and J. Han, *Trends Biotechnol.*, 2008, **26**, 311.
- 13 M. Karlsson, M. Davidson, R. Karlsson, A. Karlsson, J. Bergenholtz, Z. Konkoli, A. Jesorka, T. Lobovkina, J. Hürtig, M. Voinova and O. Orwar, *Annu. Rev. Phys. Chem.*, 2004, **55**, 613.
- 14 C. L. Rice and R. Whitehead, *J. Phys. Chem.*, 1965, **69**, 4017.
- 15 J. M. Ramsey, J. P. Alarie, S. C. Jacobson and N. J. Peterson, *Proceedings of the μ TAS 2002 Symposium, 6th Nara, Japan*, Kluwer, Dordrecht, 2002, pp. 314–316.
- 16 S. Pennathur and J. G. Santiago, *Anal. Chem.*, 2005, **77**, 6772.
- 17 R. Qiao and N. R. Aluru, *Langmuir*, 2005, **21**, 8972.
- 18 R. Qiao and N. R. Aluru, *Appl. Phys. Lett.*, 2005, **86**, 143105.
- 19 S. Pennathur and J. G. Santiago, *Anal. Chem.*, 2005, **77**, 6782.
- 20 D. Stein, F. H. J. van der Heyden, W. J. A. Koopmans and C. Dekker, *Proc. Natl. Acad. Sci. U. S. A.*, 2006, **103**, 15853.
- 21 J. A. Luckey and L. M. Smith, *Electrophoresis*, 1993, **14**, 492.
- 22 J. Han, J. Fu and R. B. Schoch, *Lab Chip*, 2008, **8**, 23.
- 23 Q. Pu, J. Yun, H. Temkin and S. Liu, *Nano Lett.*, 2004, **4**, 1099.
- 24 I. Nischang, G. Chen and U. Tallarek, *J. Chromatogr., A*, 2006, **1109**, 32.
- 25 F. C. Leinweber and U. Tallarek, *Langmuir*, 2004, **20**, 11637.
- 26 I. Rubinstein and B. Zaltzman, *Phys. Rev. E*, 2000, **62**, 2238.
- 27 I. Rubinstein, B. Zaltzman, J. Pretz and C. Linder, *Russ. J. Electrochem.*, 2002, **38**, 853.
- 28 S. J. Kim, Y.-C. Wang, J. H. Lee, H. Jang and J. Han, *Phys. Rev. Lett.*, 2007, **99**, 044501.
- 29 Y. C. Wang, A. L. Stevens and J. Han, *Anal. Chem.*, 2005, **77**, 4293.
- 30 K. Zhou, M. L. Kovarik and S. C. Jacobson, *J. Am. Chem. Soc.*, 2008, **130**, 8614.
- 31 S. K. Griffiths and R. H. Nilson, *Anal. Chem.*, 1999, **71**, 5522.
- 32 S. K. Griffiths and R. H. Nilson, *Anal. Chem.*, 2006, **78**, 8134.
- 33 X. Xuan and D. Li, *Electrophoresis*, 2007, **28**, 627.
- 34 A. De Leebeeck and D. Sinton, *Electrophoresis*, 2006, **27**, 4999.
- 35 X. Xuan, *Anal. Chem.*, 2007, **79**, 7928.
- 36 D. Dutta, *Electrophoresis*, 2007, **28**, 4552.
- 37 D. Dutta, *Anal. Chem.*, 2008, **80**, 4723.
- 38 X. Xuan, *J. Chromatogr., A*, 2008, **1187**, 289.
- 39 F. Baldessari, *J. Colloid Interface Sci.*, 2008, **325**, 539.
- 40 F. Baldessari, *J. Colloid Interface Sci.*, 2008, **325**, 526.
- 41 A. L. Garcia, L. K. Ista, D. N. Petsev, M. J. O'Brien, P. Bisong, A. A. Mammoli, S. R. J. Brueck and G. P. Lopez, *Lab Chip*, 2005, **5**, 1271.
- 42 Y.-J. Oh, A. L. Garcia, D. N. Petsev, G. P. Lopez, S. R. J. Brueck, C. F. Ivory and S. M. Han, *Lab Chip*, 2009, **9**, 1601.
- 43 S. Das and S. Chakraborty, *Electrophoresis*, 2008, **29**, 1115.
- 44 S. Das and S. Chakraborty, *Langmuir*, 2008, **24**, 7704.
- 45 S. Pennathur, F. Baldessari, J. G. Santiago, M. G. Kattah, J. B. Steinman and P. J. Utz, *Anal. Chem.*, 2007, **79**, 8316.
- 46 J. Han and H. G. Craighead, *J. Vac. Sci. Technol., A*, 1999, **17**, 2142.
- 47 J. Han and H. G. Craighead, *Science*, 2000, **288**, 1026.
- 48 J. Fu, P. Mao and J. Han, *Appl. Phys. Lett.*, 2005, **87**, 263902.
- 49 J. Fu, R. B. Schoch, A. L. Stevens, S. R. Tannenbaum and J. Han, *Nat. Nanotechnol.*, 2007, **2**, 121.
- 50 P. Mao and J. Han, *Lab Chip*, 2009, **9**, 586.
- 51 M. Tabuchi, M. Ueda, N. Kaji, Y. Yamasaki, Y. Nagasaki, K. Yoshikawa, K. Kataoka and Y. Baba, *Nat. Biotechnol.*, 2004, **22**, 337.
- 52 Y. Zeng and D. J. Harrison, *Anal. Chem.*, 2007, **79**, 2289.
- 53 N. Kaji, Y. Tezuka, Y. Takamura, M. Ueda, T. Nishimoto, H. Nakanishi, Y. Horiike and Y. Baba, *Anal. Chem.*, 2004, **76**, 15.
- 54 J. Shi, A. P. Fang, L. Malaquin, A. Pepin, D. Decanini, J. L. Viovy and Y. Chen, *Appl. Phys. Lett.*, 2007, **91**, 153114.
- 55 C.-W. Kuo, K. H. Wei, C.-H. Lin, J.-Y. Shiu and P. Chen, *Electrophoresis*, 2008, **29**, 2931.
- 56 B. Y. Kim, J. Yang, M. Gong, B. R. Flachsbarth, M. A. Shannon, P. W. Bohn and J. V. Sweedler, *Anal. Chem.*, 2009, **81**, 2715.
- 57 D. P. Wernette, C. B. Swearingen, D. M. Crokek, Y. Lu, J. V. Sweedler and P. W. Bohn, *Analyst*, 2006, **131**, 41.
- 58 Z. Siwy, L. Trofin, P. Kohli, L. A. Baker, C. Trautmann and C. R. Martin, *J. Am. Chem. Soc.*, 2005, **127**, 5000.
- 59 S. B. Lee, D. T. Mitchell, L. Trofin, T. K. Nevanen, H. Soderlund and C. R. Martin, *Science*, 2002, **296**, 2198.
- 60 V. P. Menon and C. R. Martin, *Anal. Chem.*, 1995, **67**, 1920.
- 61 C. R. Martin, M. Nishizawa, K. Jirage and M. Kang, *J. Phys. Chem. B*, 2001, **105**, 1925.
- 62 B. Y. Kim, C. B. Swearingen, J. A. Ho, E. V. Romanova, P. W. Bohn and J. V. Sweedler, *J. Am. Chem. Soc.*, 2007, **129**, 7620.
- 63 A. Piruska, S. Branagan, D. M. Crokek, J. V. Sweedler and P. W. Bohn, *Lab Chip*, 2008, **8**, 1625.
- 64 M. Gershow and J. A. Golovchenko, *Nat. Nanotechnol.*, 2007, **2**, 775.
- 65 J. J. Kasianowicz, E. Brandin, D. Branton and D. W. Deamer, *Proc. Natl. Acad. Sci. U. S. A.*, 1996, **93**, 13770.
- 66 H. Bayley and C. R. Martin, *Chem. Rev.*, 2000, **100**, 2575.
- 67 S. G. Lemay, *ACS Nano*, 2009, **3**, 775.
- 68 S. E. Henrickson, M. Misakian, B. Robertson and J. J. Kasianowicz, *Phys. Rev. Lett.*, 2000, **85**, 3057.
- 69 S. M. Bezrukov, I. Vodyanoy and V. A. Parsegian, *Nature*, 1994, **370**, 279.
- 70 A. Meller, L. Nivon, E. Brandin, J. Golovchenko and D. Branton, *Proc. Natl. Acad. Sci. U. S. A.*, 2000, **97**, 1079.
- 71 J. Mathé, A. Aksimentiev, D. R. Nelson, K. Schulten and A. Meller, *Proc. Natl. Acad. Sci. U. S. A.*, 2005, **102**, 12377.
- 72 L. Song, M. R. Hobaugh, C. Shustak, S. Cheley, H. Bayley and J. E. Gouaux, *Science*, 1996, **274**, 1859.
- 73 M. Akeson, D. Branton, J. J. Kasianowicz, E. Brandin and D. W. Deamer, *Biophys. J.*, 1999, **77**, 3227.
- 74 A. Meller, L. Nivon and D. Branton, *Phys. Rev. Lett.*, 2001, **86**, 3435.
- 75 W. Vercootere, S. Winters-Hilt, H. Olsen, D. Deamer, D. Haussler and M. Akeson, *Nat. Biotechnol.*, 2001, **19**, 248.
- 76 T. Z. Butler, J. H. Gundlach and M. T. Roll, *Biophys. J.*, 2007, **93**, 3229.
- 77 K. V. Voelkerding, S. A. Dames and J. D. Durtschi, *Clin. Chem. (Washington, D. C.)*, 2009, **55**, 641.
- 78 M. Rhee and M. A. Burns, *Trends Biotechnol.*, 2006, **24**, 580.
- 79 D. Branton, D. W. Deamer, A. Marziali, H. Bayley, S. A. Benner, T. Butler, M. Di Ventra, S. Garaj, A. Hibbs, X. Huang, S. B. Jovanovich, P. S. Krstic, S. Lindsay, X. S. Ling, C. H. Mastrangelo, A. Meller, J. S. Oliver, Y. V. Pershin, J. M. Ramsey, R. Riehn, G. V. Soni, V. Tabard-Cossa, M. Wanunu, M. Wiggins and J. A. Schloss, *Nat. Biotechnol.*, 2008, **26**, 1146.
- 80 T. Z. Butler, J. H. Gundlach and M. A. T. Roll, *Biophys. J.*, 2006, **90**, 190.
- 81 S. Winters-Hilt, E. Morales, I. Amin and A. Stoyanov, *BMC Bioinf.*, 2007, **8**, S20.
- 82 J. W. F. Robertson, C. G. Rodrigues, V. M. Stanford, K. A. Rubinson, O. V. Krasinikov and J. J. Kasianowicz, *Proc. Natl. Acad. Sci. U. S. A.*, 2007, **104**, 8207.
- 83 B. C. Gierhart, D. G. Howitt, S. J. Chen, Z. Zhu, D. E. Kotecki, R. L. Smith and S. D. Collins, *Sens. Actuators, B*, 2008, **132**, 593.
- 84 J. Li, D. Stein, C. McMullan, D. Branton, M. J. Aziz and J. A. Golovchenko, *Nature*, 2001, **412**, 166.
- 85 O. A. Saleh and L. L. Sohn, *Nano Lett.*, 2003, **3**, 37.
- 86 D. Fologea, M. Gershow, B. Ledden, D. S. McNabb, J. A. Golovchenko and J. Li, *Nano Lett.*, 2005, **5**, 1905.
- 87 M. Wanunu, J. Sutin, B. McNally, A. Chow and A. Meller, *Biophys. J.*, 2008, **95**, 4716.
- 88 A. Han, G. Schurmann, G. Mondin, R. A. Bitterli, N. G. Hegelbach, N. F. de Rooij and U. Staufer, *Appl. Phys. Lett.*, 2006, **88**, 093901.

- 89 Y. Choi, L. A. Baker, H. Hillebrenner and C. R. Martin, *Phys. Chem. Chem. Phys.*, 2006, **8**, 4976.
- 90 J. E. Wharton, P. Jin, L. T. Sexton, L. P. Horne, S. A. Sherrill, W. K. Mino and C. R. Martin, *Small*, 2007, **3**, 1424.
- 91 E. A. Heins, Z. S. Siwy, L. A. Baker and C. R. Martin, *Nano Lett.*, 2005, **5**, 1824.
- 92 C. C. Harrell, Y. Choi, L. P. Horne, L. A. Baker, Z. S. Siwy and C. R. Martin, *Langmuir*, 2006, **22**, 10837.
- 93 K. B. Jirage, J. C. Hulteen and C. R. Martin, *Science*, 1997, **278**, 655.
- 94 M. Nishizawa, V. P. Menon and C. R. Martin, *Science*, 1995, **268**, 700.
- 95 J. C. Hulteen, K. B. Jirage and C. R. Martin, *J. Am. Chem. Soc.*, 1998, **120**, 6603.
- 96 K. B. Jirage, J. C. Hulteen and C. R. Martin, *Anal. Chem.*, 1999, **71**, 4913.
- 97 S. B. Lee and C. R. Martin, *Anal. Chem.*, 2001, **73**, 768.
- 98 C. R. Martin and Z. S. Siwy, *Science*, 2007, **317**, 331.
- 99 S. Howorka, S. Cheley and H. Bayley, *Nat. Biotechnol.*, 2001, **19**, 636.
- 100 R. F. Purnell, K. K. Mehta and J. J. Schmidt, *Nano Lett.*, 2008, **8**, 3029.
- 101 D. Stoddart, A. J. Heron, E. Mikhailova, G. Maglia and H. Bayley, *Proc. Natl. Acad. Sci. U. S. A.*, 2009, **106**, 7702.
- 102 L.-J. Cheng and L. J. Guo, in *Ion-Current Rectification in Nanofluidic Devices*, ed. J. B. Edel and A. J. deMello, RSC Publishing, Cambridge, 2009, pp. 157–177.
- 103 R. Karnik, C. Duan, K. Castelino, H. Daiguji and A. Majumdar, *Nano Lett.*, 2007, **7**, 547.
- 104 I. Vlasiouk, S. Smirnov and Z. Siwy, *ACS Nano*, 2008, **2**, 1589.
- 105 X. Wang, J. Xue, L. Wang, W. Guo, W. Zhang, Y. Wang, Q. Liu, H. Ji and Q. Ouyang, *J. Phys. D: Appl. Phys.*, 2007, **40**, 7077.
- 106 D. Constantin and Z. S. Siwy, *Phys. Rev. E*, 2007, **76**, 041202.
- 107 H. Daiguji, Y. Oka and K. Shirono, *Nano Lett.*, 2005, **5**, 2274.
- 108 A. Alcaraz, P. Ramirez, E. Garcia-Gimenez, M. L. Lopez, A. Andrio and V. M. Aguilera, *J. Phys. Chem. B*, 2006, **110**, 21205.
- 109 M. Ali, P. Ramirez, S. Mafé, R. Neumann and W. Ensinger, *ACS Nano*, 2009, **3**, 603.
- 110 Y. He, D. Gillespie, D. Boda, I. Vlasiouk, R. S. Eisenberg and Z. S. Siwy, *J. Am. Chem. Soc.*, 2009, **131**, 5194.
- 111 I. Vlasiouk, T. R. Kozel and Z. S. Siwy, *J. Am. Chem. Soc.*, 2009, **131**, 8211.
- 112 R. Karnik, R. Fan, M. Yue, D. Li, P. Yang and A. Majumdar, *Nano Lett.*, 2005, **5**, 943.
- 113 R. Karnik and K. Castelino, *Appl. Phys. Lett.*, 2006, **88**, 123114.
- 114 H. Daiguji, T. Adachi and N. Tatsumi, *Phys. Rev. E*, 2008, **78**, 026301.
- 115 L.-J. Cheng and L. J. Guo, *ACS Nano*, 2009, **3**, 575.
- 116 M. J. Levene, J. Korlach, S. W. Turner, M. Foquet, H. G. Craighead and W. W. Webb, *Science*, 2003, **299**, 682.
- 117 J. T. Mannion and H. G. Craighead, *Biopolymers*, 2007, **85**, 131.
- 118 H.-U. G. Weier, *J. Histochem. Cytochem.*, 2001, **49**, 939.
- 119 C. Schurra and A. Bensimon, *Methods Mol. Biol. (Totowa, N. J.)*, 2009, **464**, 71.
- 120 K. T. Samiee, M. Foquet, L. Guo, E. C. Cox and H. G. Craighead, *Biophys. J.*, 2005, **88**, 2145.
- 121 K. T. Samiee, J. M. Moran-Mirabal, Y. K. Cheung and H. G. Craighead, *Biophys. J.*, 2006, **90**, 3288.
- 122 J. M. Moran-Mirabal and H. G. Craighead, *Methods*, 2008, **46**, 11.
- 123 J. M. Moran-Mirabal, A. J. Torres, K. T. Samiee, B. A. Baird and H. G. Craighead, *Nanotechnology*, 2007, **18**, 195101.
- 124 M. Foquet, K. T. Samiee, X. X. Kong, B. P. Chaudhuri, P. M. Lundquist, S. W. Turner, J. Freudenthal and D. B. Roitman, *J. Appl. Phys.*, 2008, **103**, 034301.
- 125 J. Korlach, P. J. Marks, R. L. Cicero, J. J. Gray, D. L. Murphy, D. B. Roitman, T. T. Pham, G. A. Otto, M. Foquet and S. W. Turner, *Proc. Natl. Acad. Sci. U. S. A.*, 2008, **105**, 1176.
- 126 J. Eid, A. Fehr, J. Gray, K. Luong, J. Lyle, G. Otto, P. Peluso, D. Rank, P. Baybayan, B. Bettman, A. Bibillo, K. Bjornson, B. Chaudhuri, F. Christians, R. Cicero, S. Clark, R. Dalal, A. Dewinter, J. Dixon, M. Foquet, A. Gaertner, P. Hardenbol, C. Heiner, K. Hester, D. Holden, G. Kearns, X. X. Kong, R. Kuse, Y. Lacroix, S. Lin, P. Lundquist, C. C. Ma, P. Marks, M. Maxham, D. Murphy, I. Park, T. Pham, M. Phillips, J. Roy, R. Sebra, G. Shen, J. Sorenson, A. Tomaney, K. Travers, M. Trulson, J. Vieceli, J. Wegener, D. Wu, A. Yang, D. Zaccarin, P. Zhao, F. Zhong, J. Korlach and S. Turner, *Science*, 2009, **323**, 133.
- 127 T. Miyake, T. Tani, H. Sonobe, R. Akahori, N. Shimamoto, T. Ueno, T. Funatsu and I. Ohdomari, *Anal. Chem.*, 2008, **80**, 6018.
- 128 J. B. Edel, M. Wu, B. Baird and H. G. Craighead, *Biophys. J.*, 2005, **88**, L43.
- 129 M. Gong, K. R. Wehmeyer, P. A. Limbach, F. Arias and W. R. Heineman, *Anal. Chem.*, 2006, **78**, 3730.
- 130 M. Gong, K. R. Wehmeyer, P. A. Limbach and W. R. Heineman, *Anal. Chem.*, 2006, **78**, 6035.
- 131 J. P. Quirino and S. Terabe, *Science*, 1998, **282**, 465.
- 132 M. Gong, K. R. Wehmeyer, P. A. Limbach and W. R. Heineman, *J. Chromatogr., A*, 2007, **1167**, 217.
- 133 Z. Long, Z. Shen, D. Wu, J. Qin and B. Lin, *Lab Chip*, 2007, **7**, 1819.
- 134 T. Kim and E. Meyhofer, *Anal. Chem.*, 2008, **80**, 5383.
- 135 T. C. Kuo, L. A. Sloan, J. V. Sweedler and P. W. Bohn, *Langmuir*, 2001, **17**, 6298.
- 136 Y. Zhang and A. T. Timperman, *Analyst*, 2003, **128**, 537.
- 137 T.-C. Kuo, D. M. Cannon, M. A. Shannon, P. W. Bohn and J. V. Sweedler, *Sens. Actuators, A*, 2003, **102**, 223.
- 138 A. N. Chatterjee, D. M. Cannon Jr, E. N. Gatimu, J. V. Sweedler, N. R. Aluru and P. W. Bohn, *J. Nanopart. Res.*, 2005, **7**, 507.
- 139 J. H. Lee, S. Chung, S. J. Kim and J. Han, *Anal. Chem.*, 2007, **79**, 6868.
- 140 J. H. Lee, Y.-A. Song, S. R. Tannenbaum and J. Han, *Anal. Chem.*, 2008, **80**, 3198.
- 141 S. Song, A. K. Singh and B. J. Kirby, *Anal. Chem.*, 2004, **76**, 4589.
- 142 R. S. Foote, J. Khandurina, S. C. Jacobson and J. M. Ramsey, *Anal. Chem.*, 2005, **77**, 57.
- 143 S. Song, A. K. Singh, T. J. Shepodd and B. J. Kirby, *Anal. Chem.*, 2004, **76**, 2367.
- 144 H. Daiguji, P. Yang and A. Majumdar, *Nano Lett.*, 2004, **4**, 137.
- 145 S. M. Kim, M. A. Burns and E. F. Hasselbrink, *Anal. Chem.*, 2006, **78**, 4779.
- 146 M. D. Cannon, Jr, T.-C. Kuo, P. W. Bohn and J. V. Sweedler, *Anal. Chem.*, 2003, **75**, 2224.
- 147 T. L. King, E. N. Gatimu and P. W. Bohn, *Biomicrofluidics*, 2009, **3**, 012004.
- 148 M. Gong, B. R. Flachsbarth, M. A. Shannon, P. W. Bohn and J. V. Sweedler, *Electrophoresis*, 2008, **29**, 1237.
- 149 M. Gong, B. Y. Kim, B. R. Flachsbarth, M. A. Shannon, P. W. Bohn and J. V. Sweedler, *IEEE Sens. J.*, 2008, **8**, 601.
- 150 K. Fa, J. J. Tulock, J. V. Sweedler and P. W. Bohn, *J. Am. Chem. Soc.*, 2005, **127**, 13928.
- 151 T.-C. Kuo, D. M. Cannon, Y. Chen, J. J. Tulock, M. A. Shannon, J. V. Sweedler and P. W. Bohn, *Anal. Chem.*, 2003, **75**, 1861.
- 152 V. Mengeaud, J. Jossier and H. H. Girault, *Anal. Chem.*, 2002, **74**, 4279.
- 153 D. S. Kim, S. H. Lee, T. H. Kwon and C. H. Ahn, *Lab Chip*, 2005, **5**, 739.
- 154 A. S. Kane, A. Hoffmann, P. Baumgartel, R. Seckler, G. Reichardt, D. A. Horsley, B. Schuler and O. Bakajin, *Anal. Chem.*, 2008, **80**, 9534.
- 155 M. Long, M. A. Sprague, A. A. Grimes, B. D. Rich and M. Khine, *Appl. Phys. Lett.*, 2009, **94**, 133501.
- 156 Z.-H. Wei and C.-P. Lee, *J. Appl. Phys.*, 2009, **105**, 07B523.
- 157 C.-K. Chen and C.-C. Cho, *Microfluid. Nanofluid.*, 2008, **5**, 785.
- 158 Z. Yang, H. Goto, M. Matsumoto and R. Maeda, *Electrophoresis*, 2000, **21**, 116.
- 159 T.-C. Kuo, H.-K. Kim, D. M. C. Jr, M. A. Shannon, J. V. Sweedler and P. W. Bohn, *Angew. Chem., Int. Ed.*, 2004, **43**, 1862.
- 160 X. Jin, S. Joseph, E. N. Gatimu, P. W. Bohn and N. R. Aluru, *Langmuir*, 2007, **23**, 13209.